Journal of Environmental Chemical Engineering 13 (2025) 115868

Contents lists available at ScienceDirect

Journal of Environmental Chemical Engineering

journal homepage: www.elsevier.com/locate/jece

Photodegradation of ciprofloxacin using an alginate/TiO_2 hydrogel for water remediation

Luis Hernandez Monroy [a], Jason Robert Tavares [b,*], Marie-Josée Dumont [a,*]

[a] CREPEC, département de génie chimique, Faculté des sciences et de génie, Université Laval, 2325 Rue de l'Université, Québec, QC G1V 0A6, Canada
[b] CREPEC, département de génie chimique, Polytechnique Montréal, 2500 chemin de Polytechnique, Montréal, Québec, QC H3T 1J4, Canada

ARTICLE INFO

Keywords:
Hydrogel
Antibiotic
Adsorption
Photocatalysis
Water remediation

ABSTRACT

The presence of antibiotics in aquatic environments has contributed to the emergence of multi-resistant bacteria, which can pose significant risks to human health through contaminated drinking water and food. These antibiotics enter water bodies primarily due to inefficient wastewater treatment and inadequate disposal practices in hospitals, pharmaceutical industries, and households. Therefore, the development of efficient water decontamination methods, such as adsorption and photodegradation, is crucial to mitigate water pollution. In this study, a photocatalytic hydrogel composite based on sodium alginate and TiO_2 was developed for the degradation of ciprofloxacin (CIP) in water. The hydrogel composite was characterized using various analytical techniques, including scanning electron microscopy, energy-dispersive X-ray spectroscopy, Fourier-transform infrared spectroscopy, and thermogravimetric analysis. To optimize the CIP degradation process, a fractional factorial design ($2k^{5-2}$) was employed, which identified TiO_2 concentration, hydrogel dosage (g), and UV lamp distance as the most significant factors influencing degradation efficiency. The hydrogel composite's performance was assessed under varying pH conditions and CIP concentrations. Complete degradation of CIP was achieved after 300 minutes of UV exposure. Additionally, a recyclability study demonstrated the hydrogel's stability over three cycles, with 100 % CIP removal efficiency maintained in each cycle. Notably, the adsorption capacity increased from 10 % in the first cycle to 31 % in the third cycle, which may be attributed to increased porosity of the hydrogel matrix following photodegradation.

1. Introduction

The demand for fresh water has increased significantly over the years. However, this demand often exceeds the supply needed for maintaining human health and other necessities. In addition, different pollutants have been found in fresh water. Pharmaceuticals for example have been detected in rivers due to their release from various sources[1]. These include wastewater effluents from pharmaceutical companies with inadequate treatment processes[2,3], discharge from hospitals due to human excretion[4,5] and household waste. Such pharmaceuticals, particularly antibiotics, can negatively impact aquatic ecosystems, affecting both the macro and microbiota[6]. For example, the presence of antibiotics in water can lead to the development of antibiotic-resistant bacteria[7]. Ciprofloxacin hydrochloride (CIP) is a member of the fluoroquinolone class, which is widely used against a broad spectrum of bacterial infections. It acts by binding to and inhibiting bacterial topoisomerases, thus preventing bacterial replication and leading to cell death[1], [8]. Recent studies have shown a strong correlation between the use of fluoroquinolones, such as CIP, and the emergence of resistant strains of *Escherichia coli*. For instance, CIP-resistant *E. coli* has been detected in surfers exposed to coastal water in the UK, posing a significant public health risk[9]

The concern over emerging water pollutants has driven the development of various remediation techniques. Among them, adsorption is a simple, versatile, and cost-efficient approach to capture contaminants [10]. Hydrogels have been employed as adsorbents for antibiotics in water due to their high swelling capacity, affinity for different functional groups, and decontamination ability[11]. Nevertheless, the adsorbed contaminants require subsequent treatment for degradation[12].

To address this challenge, photocatalysis has emerged as a promising solution for the degradation of adsorbed pollutants. Photocatalysis is an environmentally friendly and efficient approach that involves the use of UV light and a semiconductor-based, photo-responsive catalyst[5], [11], [13]. A photocatalyst can convert the UV component of sunlight or

* Corresponding authors.
E-mail addresses: jason.tavares@polymtl.ca (J.R. Tavares), marie-josee.dumont@gch.ulaval.ca (M.-J. Dumont).

https://doi.org/10.1016/j.jece.2025.115868
Received 16 December 2024; Received in revised form 15 February 2025; Accepted 17 February 2025
Available online 18 February 2025

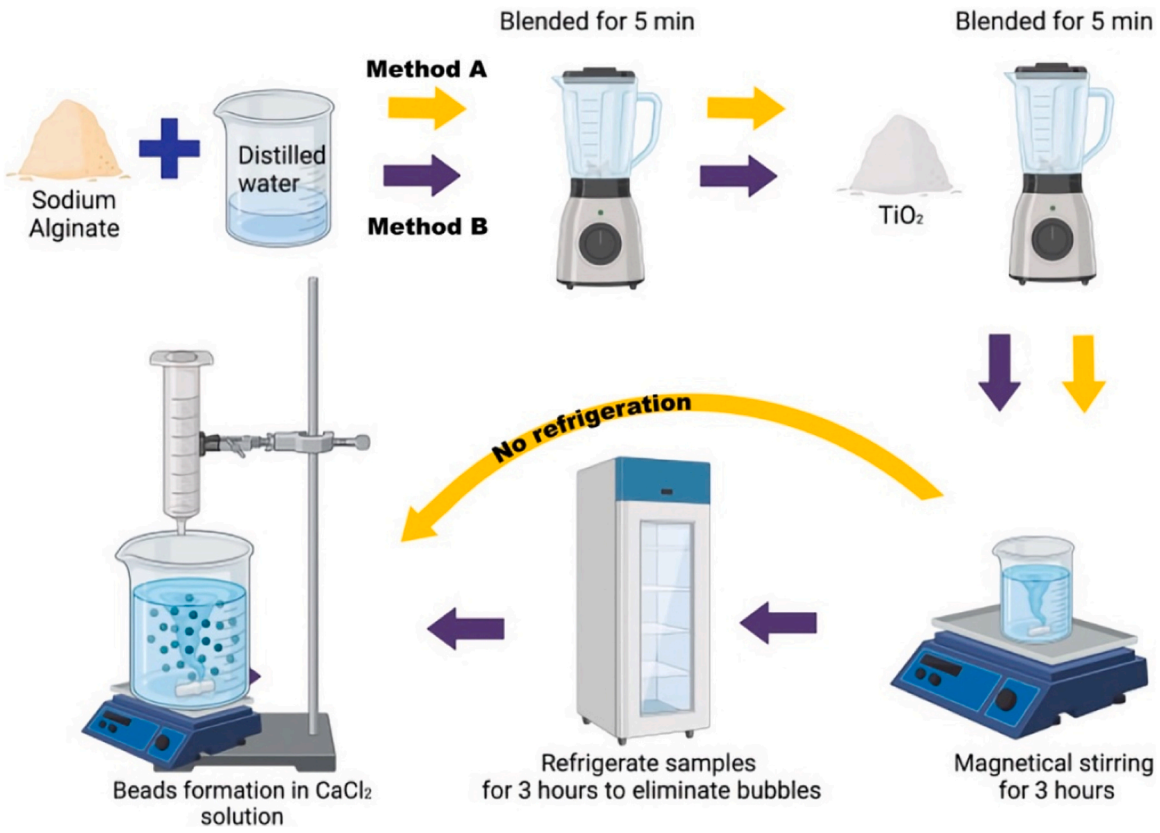

Fig. 1. Preparation of SA/TiO_2 hydrogel beads.

artificial light to initiate an advanced oxidation process (AOP)[14]. Upon activation by light, the photocatalyst generates electron (e^-) - hole (h^+) pairs that lead to the formation of superoxide radicals, which ultimately degrade contaminants into smaller molecules like CO_2 and H_2O.

Photocatalysts have been widely utilized for the degradation of various organic pollutants, including antibiotics such as sulfamethoxazole, trimethoprim, and hematoxylin[5], [15]. Some examples of photocatalysts include carbon-based catalysts, bismuth, silver, metal sulfides (MS_x), and metal oxide (MO_x). Among the MO_x catalyst, MgO, Cu_2O, Pr_6O_{11}, $MgFe_2O_4$, and TiO_2, have been successfully employed for the degradation of dyes, pharmaceuticals and others. For instance, a mullite-Pr_6O_{11} composite was prepared for methylene blue (MB) and rhodamine b (RhB) demonstrating up to 75 % degradation of a 100 mg/L contaminant solution, with good recyclability. However, Pr_6O_{11} is a rare metal oxide, making its large-scale application costly. As a result, other more abundant MO_x catalysts such as Mg, Fe, Ti, and Zn based oxides have been explored as cost-effective alternatives[16], [17], [18], [19].

In nanoparticle form, photocatalysts offer a high surface area, allowing for more efficient degradation of contaminants under light exposure [20]. However, the main challenge with using nanoparticles is their recovery post-treatment. To overcome this limitation, a $MgFe_2O_4$ .graphene composite was used for MB degradation. Due to its small particle size, 98 % degradation was achieved within 15 minutes, and due to its magnetic properties, it was successfully recovered from the reaction solution using a magnet [21].

Another option for improving recovery is the immobilization of photocatalysts within different matrices, including hydrogels, taking advantage of their adsorption properties. For instance, immobilizing TiO_2 within a hydrogel matrix offers a reliable solution, combining the benefits of adsorption to trap contaminants with photocatalysis for their degradation [22], [23], [24]. Titanium dioxide (TiO_2) is one the most widely studied photocatalysts due to its affordability, non-toxicity to humans, and photochemical stability. TiO_2 exists in three polymorphic forms: anatase, rutile, and brookite. Degussa P25 is a blend of anatase and rutile, which together exhibit a synergistic effect that enhances photocatalytic activity [25]. For example, it has been reported that TiO_2 loaded in a matrix composed of cellulose for the adsorption and degradation of tetracycline and rhodamine B dye (RhB), reached a degradation of > 95 % of the contaminants[26]. In another example, the full degradation of tetracycline was achieved using a TiO_2-poly(acrylic acid) nanocomposite; however, the use of non-degradable hydrogels can become a secondary source of contamination [27]. As an alternative, biodegradable non-toxic hydrogels can be used to load the semiconductors. For example, alginate is a polysaccharide derived from the cell walls of brown algae, is composed of β-D-mannuronic acid and α-L-guluronic acid. It exhibits excellent properties for sustainable hydrogel synthesis, such as non-toxicity, biodegradability, and biocompatibility, making it a suitable candidate for adsorbing organic pollutants, including dyes, heavy metals, and pharmaceuticals from water [28], [29], [30].

The aim of this research was to prepare a composite comprised of a hydrogel matrix to adsorb contaminants, and an abundant and non-toxic photocatalyst for the degradation of antibiotics in water. In this case, the use of sodium alginate was chosen due to its abundance, low cost and environmentally friendly properties. The integration of adsorption with photocatalysis enhanced the degradation of ciprofloxacin (CIP), providing potentially an efficient and sustainable water treatment solution.

2. Materials and methods

2.1. Materials

All chemicals were used as received from their respective suppliers. Alginic acid was obtained from MP biomedicals, while titanium dioxide

Table 1
Proportions of SA and TiO_2 for hydrogel beads preparation.

Hydrogel code	SA/TiO_2 (0 %)	SA/TiO_2 (10 %)	SA/TiO_2 (20 %)	SA/TiO_2 (30 %)
Sodium alginate (g)	2.5	2.5	2.5	2.5
TiO_2 (g)	0	0.25	0.5	0.75
Water (mL)	100	100	100	100

• (0, 10, 20, 30 %) accounts for the mass percent of TiO_2 with respect to SA.

P25 with a ratio (anatase: rutile 85:15, particle size 10–40 nm) was purchased from ACS Material. Calcium chloride (≥ 93.0 %) and the ciprofloxacin hydrochloride USP reference standard were purchased from (Sigma-Aldrich). Acetonitrile and o-phosphoric acid were supplied by Fisher Chemical, and triethylamine was obtained from Oakwood Chemical. The UV lamp (Evoluchem LED, 365 nm, 18 W, 30 degrees angle, 20 mW/cm^2 relative irradiance measured in the PhotoRedOx Box™) was purchased from HepatoChem. Additionally, ciprofloxacin tablets were obtained from a local pharmacy for photodegradation testing.

2.2. Synthesis of SA/TiO_2 beads

The synthesis of hydrogels was adapted from Zhao et al. [31] and illustrated in Fig. 1. 2.5 g of sodium alginate (SA) and 100 mL of distilled (DI) water were mixed using a common blender (one speed level, from Hamilton beach) for 5 min, and thereafter, a certain quantity of TiO_2 was added and homogenized for another 5 min (Table 1). The suspension was magnetically stirred for 3 h at 500 rpm to ensure TiO_2 homogeneity and lumps elimination. To prepare the hydrogel beads, the SA/TiO_2 suspension was added dropwise to a 0.1 M $CaCl_2$ solution using a 60 mL syringe with a 2 mm tip diameter (Method A). Alternatively, before bead formation, the suspension was stored for 3 h at 4 °C to eliminate any trapped bubbles from the suspension (Method B). The hydrogel beads were maintained overnight in a $CaCl_2$ solution to settle. Subsequently, the hydrogel beads were rinsed with DI water for 10 min to remove excess $CaCl_2$ and thereafter, stored in DI water at 4 °C until use.

2.3. Point of zero charge

The determination of the point of zero charge (PZC) was adapted from Myint et al.[32]. The test was performed in DI water adjusted to different pH from 3.0 to 13.0 using HCl and NaOH solutions and a pH meter (Thermo Electro Orion 710 A). In 50 mL falcon tubes, 0.5 g of wet hydrogel beads were added to the previously adjusted solutions. The samples were mixed using a mechanical shaker at 100 rpm for 24 h at room temperature. The final pH of the sample was measured. The PZC was determined by plotting the change in pH (Δ pH) vs the initial pH.

2.4. Ciprofloxacin tablets quantification

The antibiotic tablets (ciprofloxacin hydrochloride, 500 mg) used in this study were quantified by HPLC (Agilent 1260 infinity, Software OpenLAB), to determine the exact amount of ciprofloxacin per tablet, and the presence of possible degradation products before the photocatalysis experiments. The quantification method was adapted from United States Pharmacopeia (USP) 2023 guidelines[33]. A calibration curve was carried out using Ciprofloxacin hydrochloride USP reference standard to ensure the accuracy of the results. The mobile phase consisted of acetonitrile and phosphate buffer pH 3.0 (13:87) ratio. The phosphate buffer was prepared using a solution of phosphoric acid 0.025 M, adjusted to pH 3.0 with triethylamine. The HPLC analysis was conducted using a Gemini 5 u C18 110 A column (150 ×4.60 mm, Phenomenex) at 30 °C, with the UV detector set to a wavelength of 278 nm. The flow rate was set at 1 mL/min and the retention time of ciprofloxacin was 7 min.

Table 2
Tested factors in the 2 K^{5-2} fractional factorial design.

Parameters	Low (− 1)	Central (0)	High (+ 1)
Stirring speed (rpm)	100	350	500
Preparation method	Method A	Method A or B[a]	Method B
Hydrogel weight (g)	0.5	1.25	2
TiO_2 concentration (%)	0	10	20
UV lamp distance (cm)	10	15	20

[a] To test the central points, four tests were performed. Two experiments utilizing the method A and two experiments using method B.

To determine the amount of ciprofloxacin per tablet, the average weight per tablet was obtained, and a sample solution was prepared using the powder of 10 grinded tablets according to Eq. 1. An aliquot was taken to obtain a sample solution that fell inside the calibration curve and the valorization was obtained according to Eq. 2[33].

$$Cm = \frac{Pp * Cip}{Dose} \quad (1)$$

C_m - Amount of powdered tablet (mg) equivalent to desired amount of ciprofloxacin
P_p – Average of the tablet's weight (mg/tablet)
C_{ip} – Desired amount of pure ciprofloxacin in mg
Dose - Dose of ciprofloxacin on the label in mg equivalent to 500 mg/tablet.

$$Result = \left(\frac{r_u}{r_s}\right) * \left(\frac{C_s}{C_u}\right) * 100 \quad (2)$$

r_u = peak area from the *sample solution*
r_s = peak area from the *standard solution*
c_s = concentration of USP ciprofloxacin hydrochloride in the *standard solution* (mg/mL)
c_u = concentration of ciprofloxacin hydrochloride in the *sample solution* (mg/mL)

The acceptance criteria of CIP is 98.0 % - 102.0 % according to USP.

2.5. Adsorption-photocatalysis of ciprofloxacin in SA/TiO_2 hydrogel beads

The adsorption-photocatalysis experiments were conducted in two phases to observe the effect of adsorption of ciprofloxacin and its photodegradation separately. SA/TiO_2 hydrogel beads were added to 50 mL of tablets solution, corresponding to a known concentration of CIP. The adsorption phase was conducted under stirring at different rpm according to the experimental design in dark conditions for 60 min. Following this, the photocatalysis phase was conducted exposing the sample to UV light at 365 nm for up to 360 min. Samples were taken at specific time intervals, and the ciprofloxacin concentration of samples was determined by UV spectrophotometry. A UV-1600PC Spectrophotometer (VWR) was used to perform the quantification at a wavelength of 270 nm, using DI water as a blank[34]. A calibration curve of ciprofloxacin hydrochloride USP reference standard was carried out to ensure the accuracy of the results.

To evaluate the effect of different variables and to optimize the experimental set-up, a fractional factorial design 2 K^{5-2} was used. This type of design allows to test the main effects of various variables in only few experiments. To achieve this, only one fraction of a full factorial design is tested. Consequently, some main effects are confounded with interactions, and the corresponding slope (**β**) is a combination of both, the main factor and the confounded interactions. They are useful for screening the impact of many variables, in only few runs. (Table 2,

Figure S1). The experimental design matrix consisted in four continuous variables: stirring speed, hydrogel weight, TiO_2 concentration and UV lamp distance, as well as hydrogel preparation method as discrete variable. The fractional factorial design included 4 central points to test the curvature. To build the design, a full factorial design was written for *stirring* (A), *hydrogel quantity* (B) and *TiO_2 concentration* (C); while the *preparation method* was aliased with the interaction (D = AC) and the *UV lamp distance* with the interaction (E = ABC). Three levels (-1, 0 and 1) were defined for each factor. The results were evaluated using Design-Expert 7.0 software.

After optimizing the testing variables, the effect of TiO_2 concentration inside the SA/TiO_2 beads, the initial CIP concentration and the effect of pH were further evaluated. The adsorption-degradation were conducted with the UV lamp at a distance of 10 cm from the sample, and the sample was stirred at 500 rpm. 2 g of SA/TiO_2 hydrogel beads were dispersed into 50 mL of CIP tablets solution, and for the adsorption phase samples were taken every 10 min. Subsequently, the photocatalysis phase was conducted under UV light for up to 360 min, with samples taken at different time intervals. Initial concentrations of CIP of 10 mg/L, 15 mg/L and 20 mg/L were evaluated. At a fixed concentration of 15 mg/mL of CIP, the effect of pH from 3 to 9 was evaluated to study different pH values found in rivers[35]

The adsorption kinetics at different initial concentrations of CIP and different pH values was evaluated with the following Eqs. (3–6)[22,35]:

$$q_t = \frac{V * (C_i - C_t)}{m} \quad (3)$$

Where:

- q_t is the adsorption quantity (mg of CIP adsorbed per gram of hydrogel)
- C_i is initial concentration and C_t represent concentration at time "t" (mg/L) of CIP
- V is the solution volume (L)
- m is the total weight of the hydrogel (SA/TiO_2) (g).

To evaluate the kinetic behavior of the samples, pseudo-first-order (Eq.4) and second-order (Eq. 5) models were assessed:

$$In(q_e - q_t) = Inq_e - k_1 t \quad (4)$$

$$\frac{t}{q_t} = \frac{1}{k_2 * q_e^2} + \frac{t}{q_e} \quad (5)$$

Where:

- q_e (mg/g) is the equilibrated adsorption capacity.
- q_t (mg/g) is the total of adsorption at time t (s).
- the rate constant is k_1 (s^{-1}) and k_2 (g/mg*s)

The kinetics of CIP photocatalysis at different initial CIP concentrations and different pH values was evaluated with Eq. 6:

$$In[cip]_t = -k * t + In[cip]_0 \quad (6)$$

In $[cip]_t$ = natural logarithm of the concentration at time t
In $[cip]_0$ = natural logarithm of the concentration at initial time
k = rate constant of the first order reaction
t = time

2.6. Recyclability of SA/TiO_2 hydrogel beads

The recyclability of SA/TiO_2 hydrogel beads was assessed by reusing 2 g of SA/TiO_2 beads 3 times to degrade CIP. Each cycle involved an adsorption phase for 60 min, followed by a photocatalysis phase for 300 min. After each cycle, the hydrogels were rinsed with distilled water and the supernatant was tested until no CIP was detected. The SA/TiO_2 hydrogels were then stored at 4 ºC until use for the next cycle[22,28].

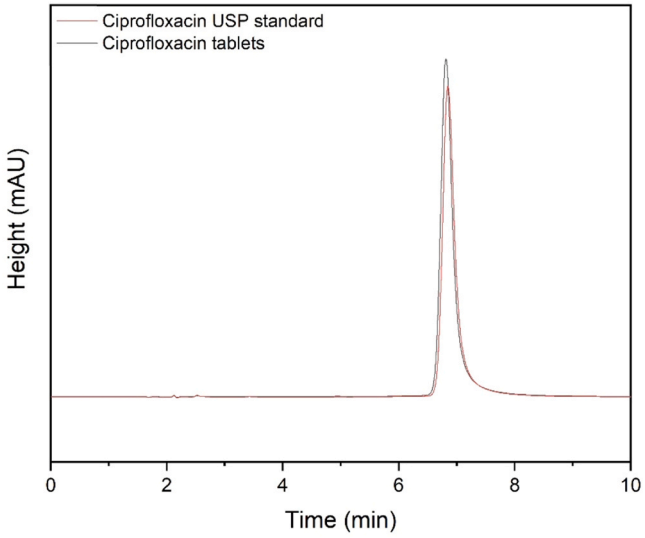

Fig. 2. Overlapped chromatograms of ciprofloxacin tablets and ciprofloxacin HCl USP standard.

2.7. Hydrogel characterization

The freshly prepared hydrogels and the samples after recyclability tests were characterized to explore their stability. Scanning electron microscopy (SEM) was used to observe the morphology of hydrogel. Using a SEM Gemini 2 Crossbeam 540 (FIB-SEM) at an accelerating voltage at 1 kV for morphology and Energy dispersive X-ray spectroscopy (SEM-EDS Inspect™ F50, Edax Ametek) at 15 kV for analysis of TiO_2 homogeneity. The samples were freeze-dried until constant weight before analysis. FT-IR spectroscopy (using a Nicolet iS50) was used to detect the presence of functional groups and to analyze chemical bonding between the alginate matrix and the embedded TiO_2 particles within the hydrogels. To execute this analysis, the samples were previously dried overnight at 80 °C in oven. A TGA (SDTA851 Mettler Toledo) was used to observe the thermal decomposition of the hydrogels. The dried samples were equilibrated at 40 °C (isothermal step 5 min). Thereafter, the samples were heated from 40 to 800 °C at a rate of 10 °C min^{-1}. X-ray diffraction test was performed to verify the crystalline form of the catalyst (Empyrean X-ray diffraction system from Malvern panalytical; Co kα1).

3. Results and discussion

3.1. Ciprofloxacin tablets quantification

A calibration curve was generated using a USP CIP standard at concentrations ranging from 0.005 to 0.03 mg/mL, demonstrating excellent linearity with a coefficient of determination (R^2) of 0.9998. The concentration of CIP in the tablets was determined by duplicate based on the calibration curve, corresponding to 98.82 % ± 0.68 % of the labeled amount of ciprofloxacin (494.1 mg of ciprofloxacin per tablet).

Furthermore, it is noteworthy that the chromatogram peaks obtained were uniform in size and shape, with no additional peaks indicating the absence of significant degradation products (Fig. 2). This suggest that the CIP in the tablets remained stable during their shelf life.

3.2. Point of zero charge of SA/TiO_2 hydrogel beads

The PZC was determined by the drift method[36]. The PZC refers to the surface state of a solid dispersed into a solution. When the solid reaches an equilibrium in between negative and positive charges on the

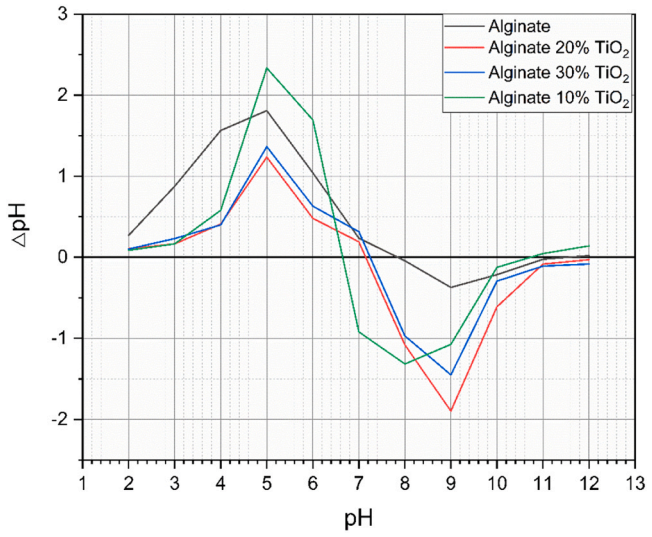

Fig. 3. PZC of SA/TiO_2 hydrogel composite.

solid surface, the surface charge is equal to zero. This parameter is essential for understanding adsorption process in pollutant removal. Depending on the electrostatic characteristics of the polymer surface, pollutants can be attracted and adsorbed, or conversely repelled[37].

The PZC (Fig. 3) is identified as the pH at which the ΔpH crosses zero. For the SA/TiO_2 (20 %) hydrogel beads, the PZC occurs at a pH of 7.2. The SA molecule is primarily composed of hydroxyl (-OH) and carboxyl functional groups ($-COO^-$)[38]. Therefore, at pH above the PZC, the surface is predominantly negatively charged due to the deprotonation of carboxyl groups, while at the PZC, the positive and negative charges are balanced, and below that point, the surface is mainly positively charged, due to protonation. The presence of cations such as Ca^{2+} and Na^+, might also play a role in the balance of charges on the hydrogel surface

3.3. Experimental design

From the fractional factorial design 2 K^{5-2} a total of eight experiments, plus central points, were conducted to the chosen design fraction. The results of each experimental run are summarized in Table 3.

An ANOVA test was performed to determine the significance of the main effects. The results are presented in Table 4. The primary factors influencing CIP degradation in descending order were TiO_2 concentration (β_C), beads method preparation (β_{AC}), hydrogel quantity (β_B), and UV lamp distance (β_{ABC}), with a significance level of $P < 0.05$.

A surface plot of the TiO_2 concentration and UV lamp distance (Figure S2 a), and TiO_2 concentration against hydrogel quantity (Figure S2 b) were carried out to provide a visualization of the factors that increased CIP degradation. It is observed that a higher TiO_2 concentration and higher hydrogel quantity help to improve CIP degradation, while a lower lamp distance is beneficial for higher degradation due to the higher irradiance, according to Eq. 7.

$$I = \frac{k}{r^2} \tag{7}$$

I = Radiation intensity
r = Distance
k = constant

Regarding the method of preparation, storing the suspension inside a fridge helped to improve the performance of the SA/TiO_2 beads. This is because allowing the suspension to stand for some time before forming the spheres helped to eliminate the entrapped air, which might decrease the TiO_2 content per bead. Therefore, the beads prepared by method B had an improved homogeneity and, consequently, improved

Table 3
Experimental design and conditions for the fractional factorial design 2 K^{5-2} study on ciprofloxacin adsorption-degradation.

Exp	β_0	Stirring	Hydrogel quantity	TiO_2 concentration	Preparation method	UV lamp distance	Degradation
β	β_0	β_A	β_B	β_C	β_{AC}	β_{ABC}	%
effect	I	A	B	C	D	E	
1	1	−1	−1	−1	+1	−1	54.0
2	1	+1	−1	−1	−1	+1	31.9
3	1	−1	+1	−1	+1	+1	57.6
4	1	+1	+1	−1	−1	−1	55
5	1	−1	−1	+1	−1	+1	44.1
6	1	+1	−1	+1	+1	−1	85.3
7	1	−1	+1	+1	−1	−1	76.9
8	1	+1	+1	+1	+1	+1	84.3
9	1	0	0	0	−1	0	52.5
10	1	0	0	0	1	0	70.8
11	1	0	0	0	1	0	60.2
12	1	0	0	0	−1	0	67.4

Table 4
ANOVA results for the Fractional Factorial Design 2^{5-2}.

Source	Sum of Squares	Degrees of freedom	Mean Square	F-value	p-value	
Model	2728.05	5	545.61	33.97	0.0023	Significant
β_A -Stirring	71.40	1	71.40	4.45	0.1027	
β_B -Hydrogel quantity	427.78	1	427.78	26.64	0.0067	
β_C -TiO_2 concentration	1060.30	1	1060.30	66.02	0.0012	
β_{AC} -Beads method preparation	671.61	1	671.61	41.82	0.0029	
β_{ABC} -Lamp distance	355.11	1	355.11	22.11	0.0093	
Curvature	27.44	2	13.72	0.8544	0.4910	Not significant
Residual	64.24	4	16.06			
Lack of fit	28.81	2	14.41	0.8133	0.5515	Not significant
Pure Error	35.42	2	17.71			
Total	2819.73	11				

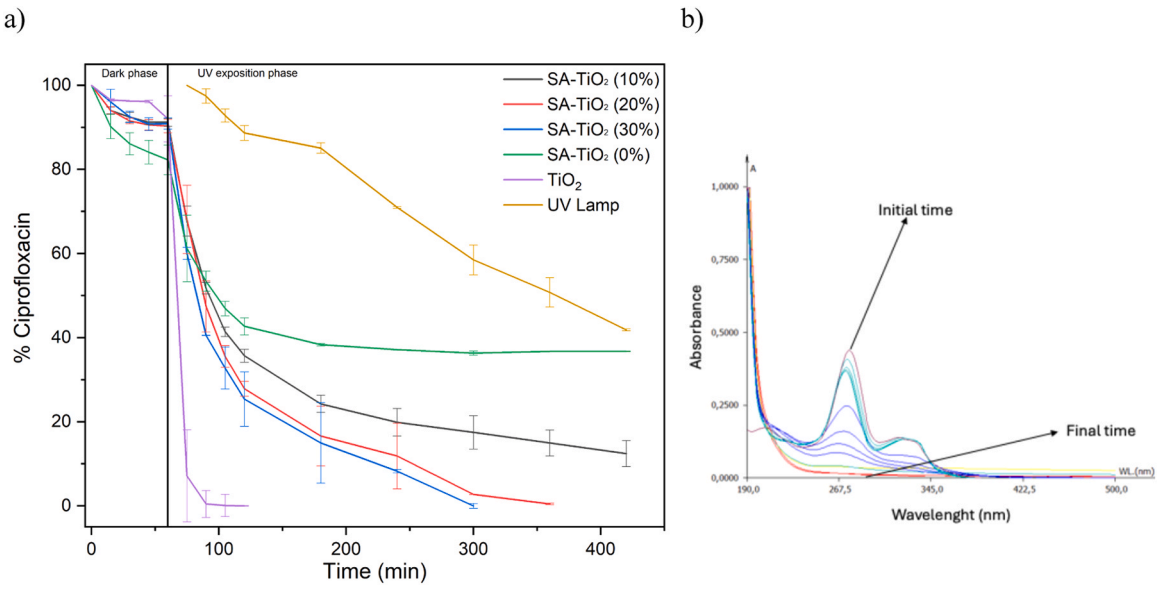

Fig. 4. a) Adsorption-photocatalysis degradation of ciprofloxacin hydrochloride of sodium alginate loaded using different concentration of TiO_2, bare TiO_2 nanoparticles, and UV light. (Conditions: UV lamp distance: 10 cm, stirring: 500 rpm, ciprofloxacin dosage: 15 mg/L, hydrogel quantity: 2 g (wet), pH 5–5.5. b) Absorbance spectra of CIP sample after adsorption and degradation by SA/TiO_2 (20 %) over time.

performance. Additionally, cooling the SA suspension prior to bead formation may have contributed to enhancing the hydrogel structure and, in turn, the strength of the beads. This effect was observed in a study where SA beads were formed at various temperatures (5–85°C). At lower temperatures, the SA beads demonstrated a more consistent internal structure with greater resistance to rupture[39]. From these results, a multilinear regression model was calculated by Design Expert 7.0 software. The following equation can be used to model CIP degradation, using the reduced, centralized variables:

Degradation (%) = 61.14 + 2.99 (Hydrogel quantity) + 11.51 (TiO_2 concentration) + 9.16 (Beads method preparation) – 6.66 (Lamp distance).

The optimal conditions obtained from this analysis were 2 g hydrogel SA/TiO_2 beads, 10 cm lamp distance, method of preparation 2, and 500 rpm for stirring. These conditions were used for the rest of the experiments, varying the TiO_2 concentration, pH and initial antibiotic concentration, since all of them can influence in the adsorption-photocatalysis process[40], [41].

3.4. *Adsorption-photocatalysis as functions of TiO_2 concentrations*

The adsorption-photocatalysis of CIP was carried out under the optimal conditions from the experimental design to evaluate the behaviour of various concentrations of TiO_2. These results were compared with bare TiO_2 and the use of UV lamp in the absence of SA/TiO_2 hydrogel beads (Fig. 4). CIP adsorption reached the equilibrium during the initial 60 min in dark conditions. In general, the adsorption was moderate. The SA/TiO_2 10 %, SA/TiO_2 20 % and SA/TiO_2 30 % adsorbed 8.8 %, 9.7 % and 9.1 % of the initial CIP, respectively, while bare TiO_2 adsorbed 7.9 % of the contaminant. The maximum CIP adsorption was 17.7 %, and it occurred when using SA beads without TiO_2. The poor adsorption of contaminant in the hydrogel may be attributed to the limited porosity of the matrix, as observed in the SEM analysis (refer to Section 3.8).

A more pronounced difference was observed during the photocatalytic phase. For instance, the CIP solution exposed to UV light in the absence of beads (thus no adsorption phase), presented a linear degradation with respect to time, resulting in 58.1 % CIP degradation after 360 min of UV exposure. A similar experiment using UV light (365 nm) in combination with hydrogen peroxide (H_2O_2) did not achieve complete CIP degradation after light exposure as reported in a previous study[42]. Interestingly, when adding hydrogel beads without TiO_2, the decrease in CIP concentration occurred faster, probably due to the adsorption of CIP in newly created pores during UV exposure as it can be observed on SEM (Fig. 9). However, an equilibrium was achieved after 180 min of exposure, resulting in 63.2 % of degradation after 360 min, which is only slightly higher than UV light without beads.

For SA loaded with TiO_2 (10 %, 20 % and 30 %), CIP degradation reached 87.5 %, 99.5 %, and 100 % respectively, with variations in the degradation time. Specifically, while the SA/TiO_2 10 % did not achieve full degradation within 360 min of UV exposure, the SA/TiO_2 20 % and SA/TiO_2 30 % achieved full degradation after 300 min and 240 min of UV exposure, respectively. In contrast, bare TiO_2 achieved full degradation within 45 min, since the interaction between contaminant-catalyst-UV light could occur faster. However, recovering TiO_2 nanoparticles can be energy-intensive and inefficient, limiting its practical application. UV absorbance spectra recorded in the range of 200 – 500 nm, showed no peaks at the final time point, suggesting the absence of conjugated bonds from the original molecule, and thus, a low likelihood of degradation products remaining in solution (Fig. 4b).

TiO_2 leaching from the hydrogel matrix was detected when using SA/TiO_2 (30 %). Studies have shown that the interaction between ionic metals and polysaccharides, such as sodium alginate, enhances metal dispersion within the matrix through the formation of coordination bonds, which follow the well-established egg-box model[43]. It is possible that, similar to Ca^{2+}, TiO_2 is also stabilized within the SA matrix through these interactions and further adsorbed via hydrogen bonding. However, an excess of catalyst may oversaturate these bonds with sodium alginate, resulting in TiO_2 not properly integrated into the matrix, which could potentially lead to leaching during photodegradation. Therefore, SA/TiO_2 (20 %) was selected for the subsequent experiments to minimize TiO_2 leaching.

The formation of active radical species through UV light exposure is responsible for the oxidation and reduction of CIP. In this process, CIP is initially adsorbed by the SA/TiO_2 hydrogel beads, possibly via hydrogen bonding between the hydroxyl groups of SA and TiOH, and the H-bond acceptors in the CIP molecule, as well as electrostatic interactions due to different charges depending on the pH (Fig. 5d) [44–46]. Subsequently, when UV light interacts with the photocatalyst inside the hydrogel, it

a)

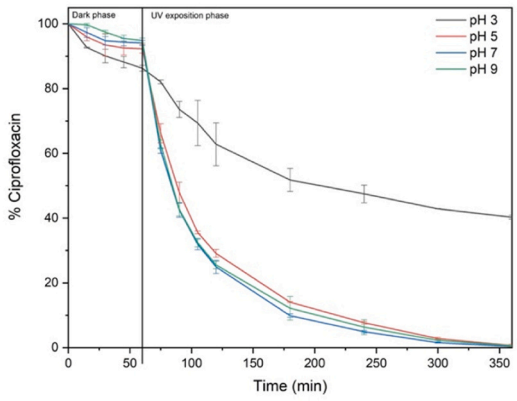

b)

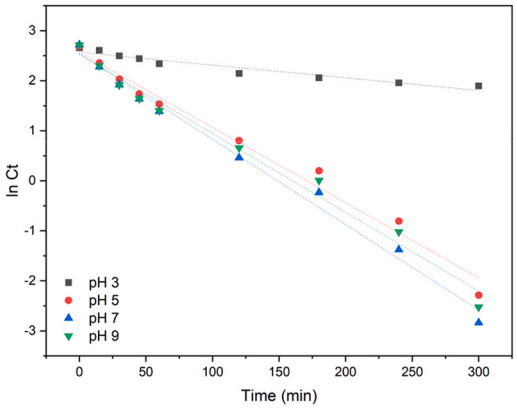

c)

	pH 3	pH 5	pH 7	pH 9
m	-0.0025	-0.0150	-0.0171	-0.0157
b	2.568	2.571	2.538	2.521
r^2	0.9310	0.9833	0.9901	0.9838
k	0.0025	0.0150	0.0171	0.0157

d)

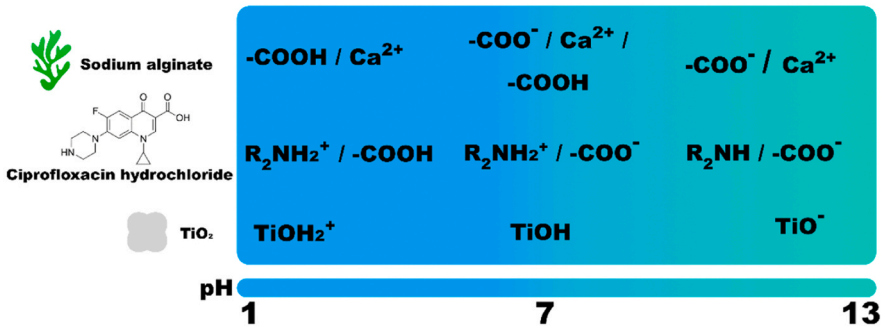

e)

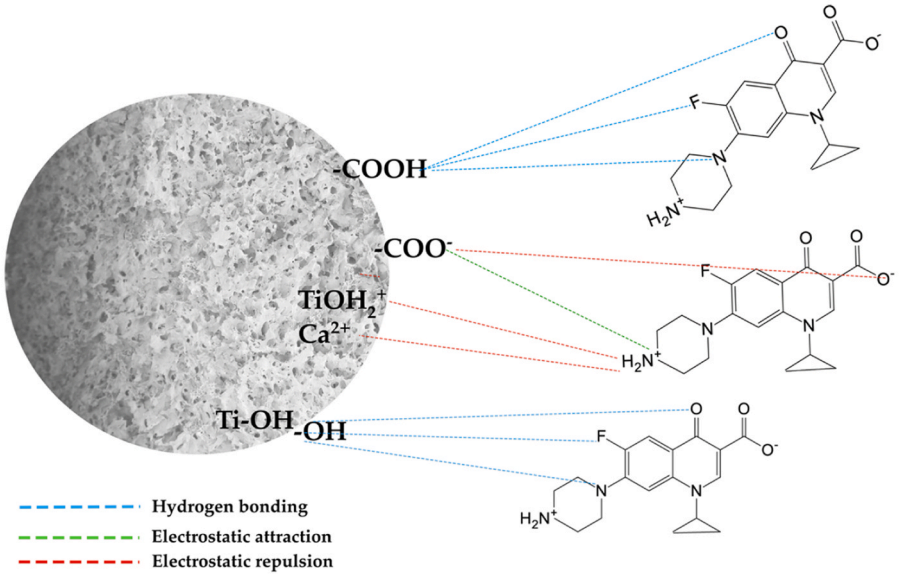

Fig. 5. a) adsorption-photocatalysis varying pH, b) and c) first-order reaction kinetics for CIP at different pH values, d) reactive species of sodium alginate, CIP and TiO_2 at different pH, and e) graphic representation of bonding sites during adsorption at pH (5 – 7).

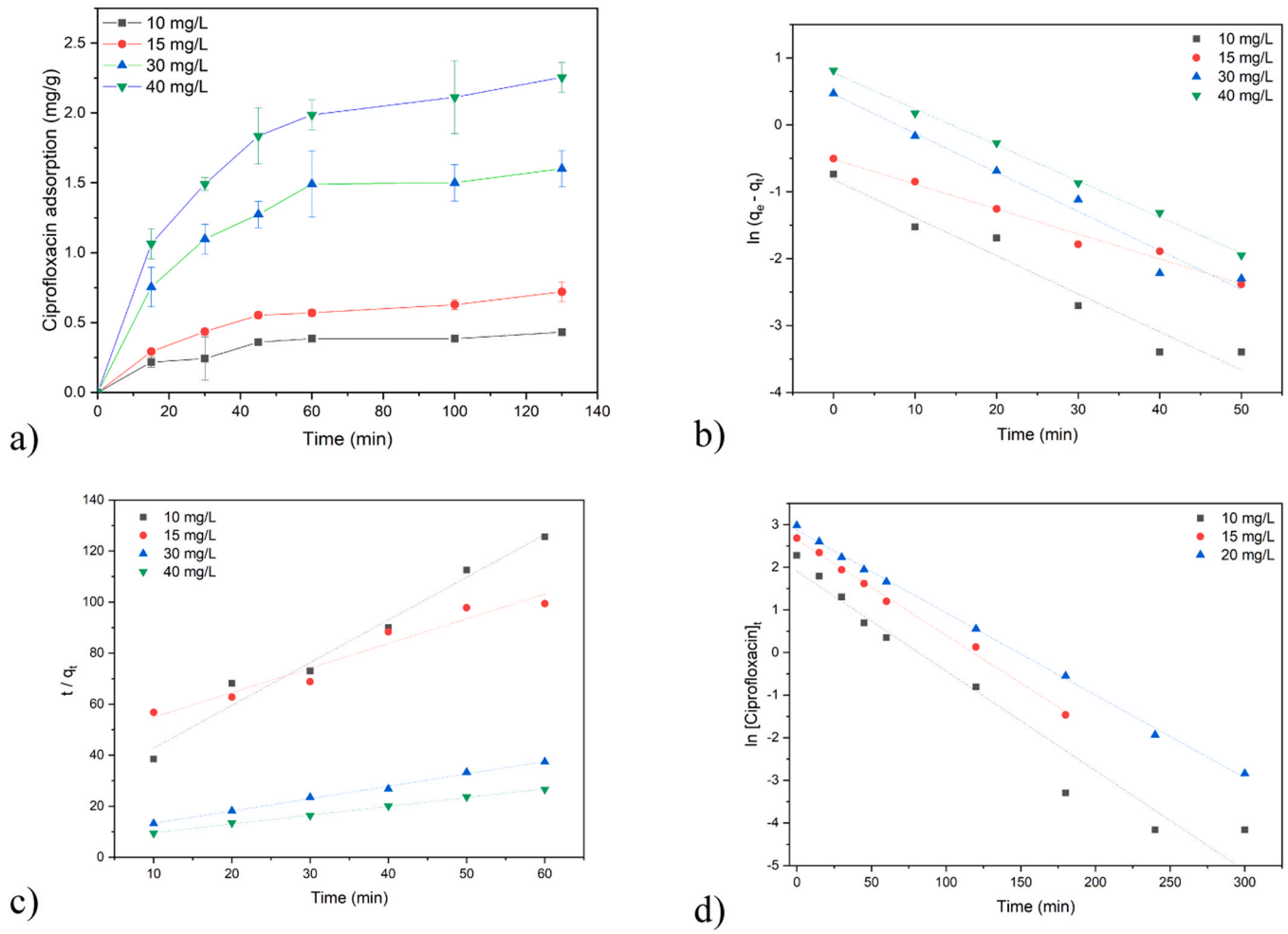

Fig. 6. a) adsorption of CIP at different concentrations, b) adsorption pseudo-first order model fitting, c) adsorption pseudo-second order model fitting and, d) first order model photocatalysis. For the adsorption of CIP, antibiotic concentration of 10, 15, 30, 40 mg/L.

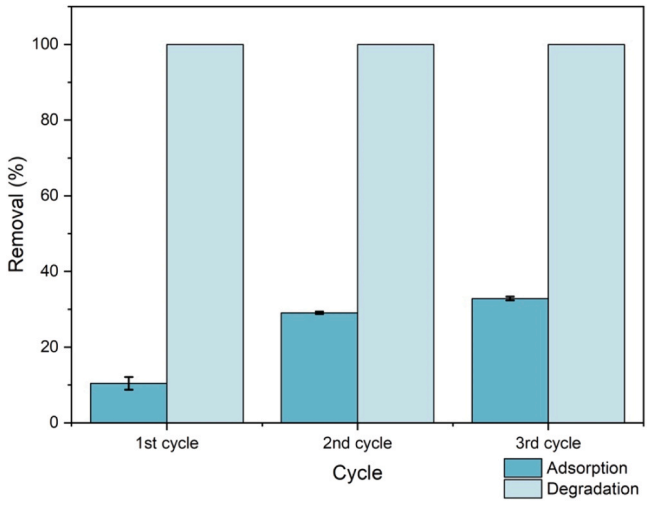

Fig. 7. Recyclability of SA/TiO_2 hydrogel composite. Error bars no visible for degradation, since the removal was 100 % in all the replicates for three cycles.

generates radical species through electron-hole migration. The holes (h^+) interact with ^-OH to create hydroxyl radicals (•OH), and the electrons interact with O_2 to create superoxide radicals ($•O_2^-$)[17], which eventually degrade CIP into smaller molecules.

3.5. *Effects of pH concentration on SA/TiO_2 hydrogel beads*

The ionic form of CIP can change at different pH values due to its two pKa values: 5.9 for the amino group and 8.89 for the carboxylic group. For instance, CIP exists as a cation (CIP+) at pH below 6, a zwitterion (CIP±) between pH 6 and 8.89, and as anion (CIP-) above 8.89. This variation in ionic forms suggests that the adsorption and degradation performance of CIP may be influenced by pH-dependent changes in its structure[47]. Similarly, pH also impacts TiO_2, which forms different surface species depending on the pH. When the pH is below the PZC of TiO_2 (pH 6.2), the dominant species in solution are $TiOH_2^+$. As the pH approaches the PZC, TiOH becomes more dominant, while at pH values above the PZC, TiO^- is the prevalent reactive species[48].

As can be observed in Fig. 5a, the degradation of ciprofloxacin significantly decreased at pH 3. This reduction could be due to electrostatic repulsion between the protonated amino group of ciprofloxacin and the positively charged $TiOH_2^+$ species during photocatalysis. In addition, as the pH increases, the concentration of hydroxyl ions (OH^-) becomes more abundant, promoting the formation of hydroxyl radicals (•OH), which enhances CIP degradation. For instance, Bismark brown dye was degraded by using different types of TiO_2. When the pH was close to the TiO_2 PZC, photodegradation reached the optimal degradation of Bismark brown dye for all the different types of TiO_2 tested[48]. The same effect was observed with the adsorption-degradation of the antibiotic oxytetracycline by TiO_2/tungsten disulfide/SA composite, in which the highest removal reported by the researchers was at pH between 6 and 7, which is close to the PZC of TiO_2[49]. In this report, the

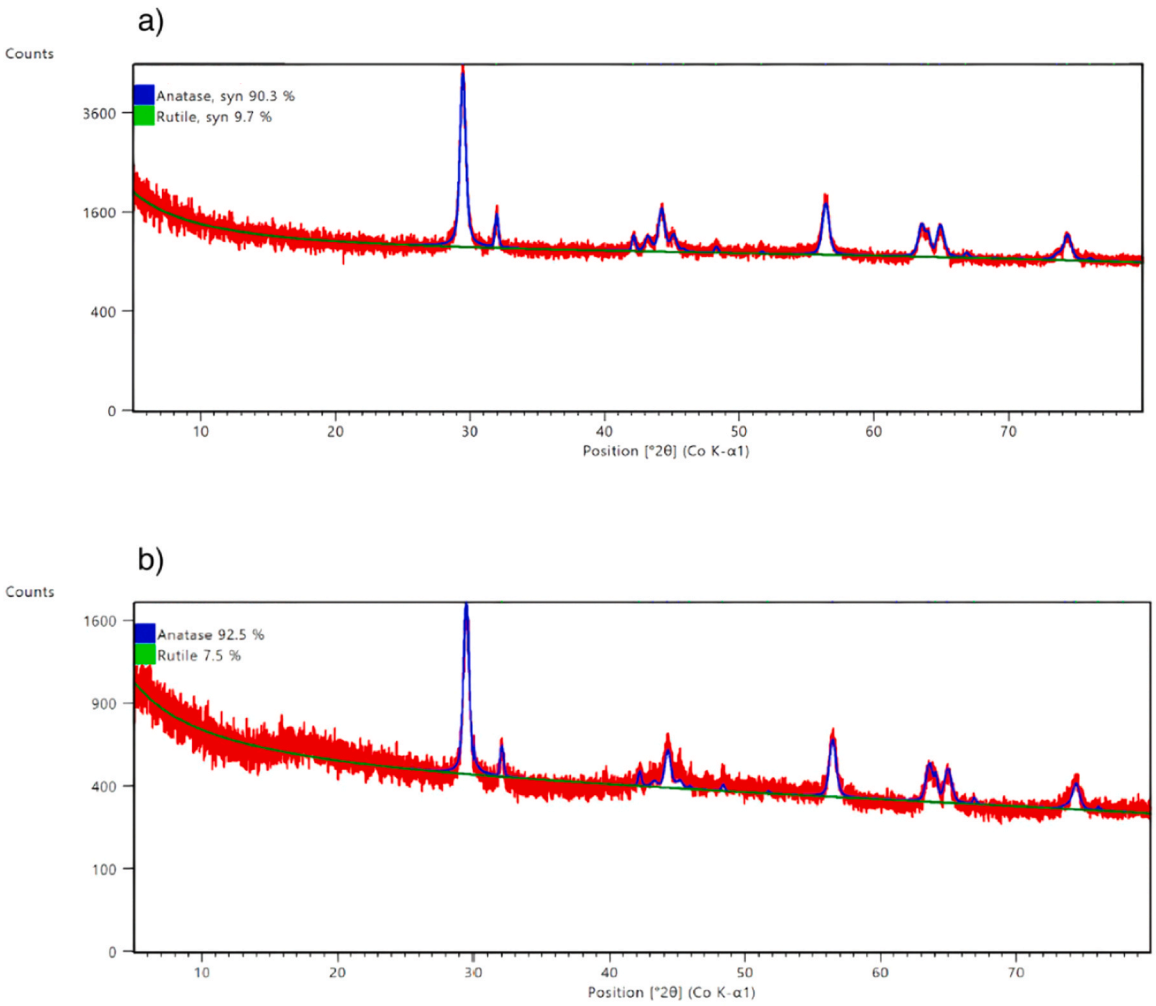

Fig. 8. XRD of a) TiO_2 reagent and b) SA/TiO_2 (20 %) hydrogel beads.

best values of degradation were observed in the pH range of 5 – 9 when using SA/TiO_2 (20 %) hydrogel beads.

The kinetic data were fitted to a first-order reaction model to determine the most suitable pH for CIP degradation with SA/TiO_2 (20 %) beads. The plot of the natural logarithm of the concentration at time t ($\ln(C_t)$) vs time (Fig. 5b) shows rate constants (k_1) of 0.0025, 0.015, 0.0171, and 0.0157 min^{-1} at pH 3, 5, 7 and 9 respectively. These results indicate that pH 7 was the most suitable for CIP degradation using SA/TiO_2 (20 %), which is closer to the PZC of TiO_2. However, due to the minimal variation in degradation rates, the pH was not controlled for the subsequent experiments as the pH of distilled water naturally falls between 5 and 6, and in the presence of CIP, the initial pH was 5.2 – 5.3.

CIP adsorption was also impacted by the pH changes, because the pH variations modify the surface charge of SA matrix as discussed in the PZC test. CIP, being a zwitterionic molecule[50], may experience repulsion when the surface charge of the adsorbent matches its charge. It has two pKa values: the first, 6.0, correspond to the basic function (amino), while the second, 8.8, is associated to the acidic function (carboxyl)[8]. Therefore, the adsorption could occur mainly through hydrogen bonding at low pH among the protonated carboxyl groups. A similar phenomenon was observed with the adsorption of another zwitterionic molecule, tetracycline, by a hydrogel composed of SA and graphene oxide. In that study, the adsorption of tetracycline reached its optimal point close to neutral (pH 6), with adsorption predominantly occurring via π- π stacking interaction and hydrogen bonds. In contrast, a reduction in tetracycline adsorption was observed at acidic and basic pH levels due to electrostatic repulsion[51].

In this case, at acidic pH, such as pH 3, the CIP might be adsorbed principally by hydrogen bonding in between carboxylic groups, carboxylic group and hydroxyl group, and amino group and carboxylic group. Another factor that could have impacted CIP adsorption is related to the ions present in the solution. For instance, at basic pH, there are abundant sodium cations due to the addition of NaOH and according to the literature, the addition of Na^+ causes the release of adsorbed CIP due to damage in the gel structure[52].

3.6. *Effect of CIP concentration on SA/TiO_2 hydrogel beads*

The adsorption of CIP onto SA/TiO_2 beads was evaluated at various initial CIP concentrations ranging from 10 to 40 mg/L at pH 5.2 – 5.3. (Fig. 6). Adsorption-desorption equilibrium was achieved within 60 min. The SA/TiO_2 hydrogel exhibited minimal variation in adsorption capacity across different initial CIP concentrations, with adsorption percentages of 10.8 %, 9.5 %, 12.4 %, and 13.2 % at 10, 15, 30, and 40 mg/L, respectively. These relatively low adsorption rates can be attributed to the weak electrostatic attraction between the hydrogel and CIP at this pH range. To further investigate the ability of the hydrogel to adsorb CIP at different concentrations, both pseudo-first order and pseudo-second order models were used to calculate the kinetic parameters. Both models showed good fitting, with $r^2 \geq 0.95$. The calculated $\boldsymbol{q_e}$ values from the pseudo-first order model were in closer agreement with the experimental $\boldsymbol{q_e}$ values, indicating that the adsorption process follows the pseudo-first-order kinetics. This indicates that adsorption

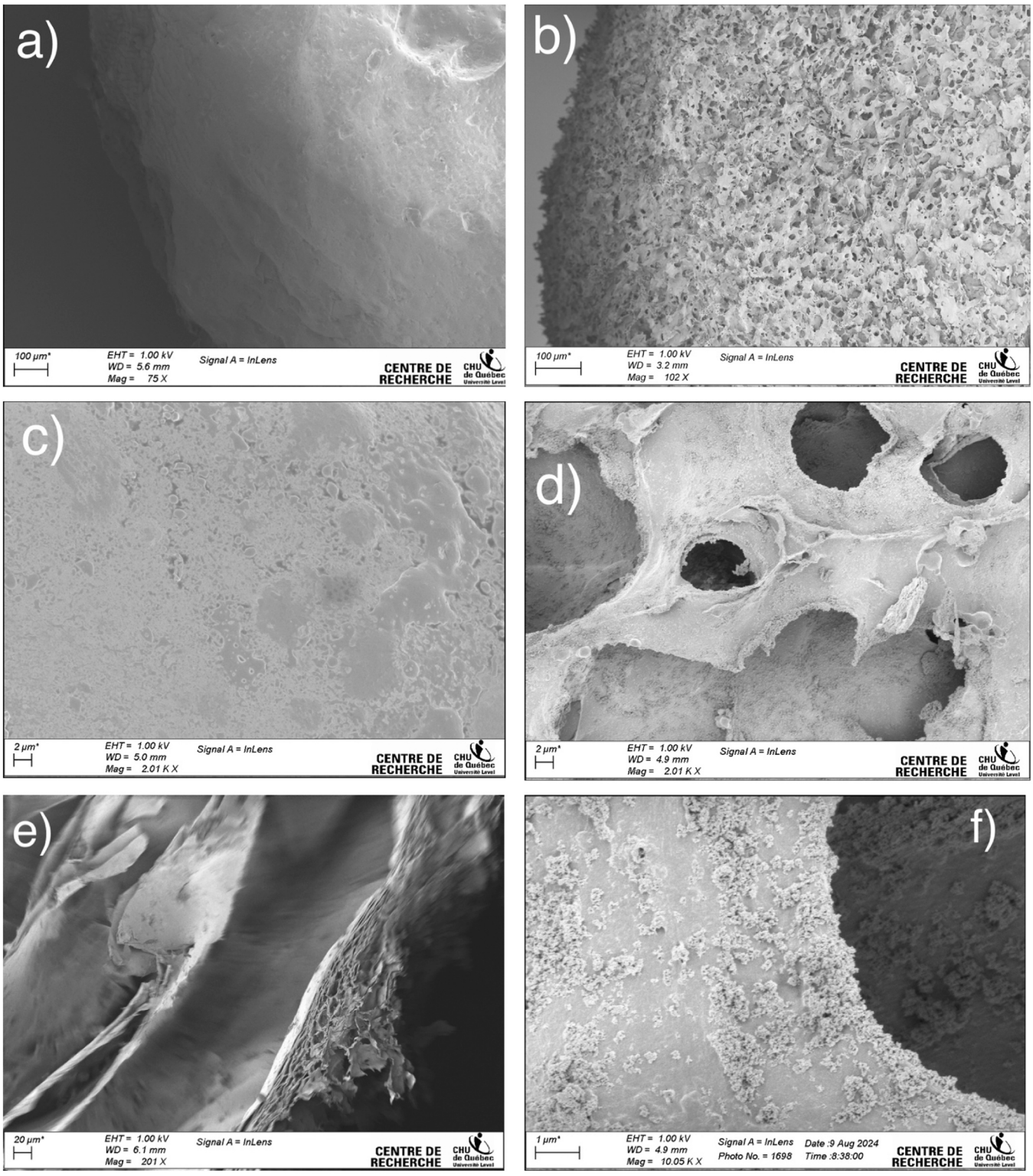

Fig. 9. SEM SA/TiO_2 hydrogel. a) and c) SA/TiO_2 (20 %) hydrogel without treatment, b) SA/TiO_2 (20 %) after three cycles of use, d) magnification of SA/TiO_2 (20 %) pores, e) transversal cut of SA/TiO_2 (20 %), and f) agglomeration of TiO_2 nanoparticles over SA matrix.

occurs predominantly in the initial stages when CIP concentrations are relatively high. Furthermore, the good fit with the pseudo-first-order model suggests that both external and internal diffusion could be the rate-limiting steps during adsorption [53]. The **k** values obtained from the pseudo-first-order model indicated that the concentration of 30 mg/L resulted in the highest k value, suggesting a faster adsorption process at this concentration (Table 5).

Following adsorption-desorption equilibrium, the CIP-loaded hydrogel was exposed to UV light for photodegradation at CIP concentrations of 10, 15 and 20 mg/L. The SA/TiO_2 hydrogel effectively degraded CIP, achieving removal efficiencies of 99.8 %, 99.5 % and 99.7 % respectively, after 300 min of light exposure. The photodegradation data indicated a first-order reaction, as per the following equation[54].

Table 5
Adsorption kinetics for CIP using SA/TiO_2 (20 %).

	Equation pseudo first order				Equation pseudo second order			
CIP concentration	10 mg/L	15 mg/L	30 mg/L	40 mg/L	10 mg/L	15 mg/L	30 mg/L	40 mg/L
m	−0.0568	−0.0372	−0.0583	−0.0539	1.672	0.9641	0.4846	0.3446
b	−0.8183	−0.5127	0.4563	0.7790	26.074	45.227	8.464	6.190
r^2	0.9514	0.9846	0.9714	0.9976	0.9758	0.9485	0.9956	0.9983
qe (cal) (mg g^{-1})	0.4411	0.5988	1.5782	2.1794	0.5978	1.0371	2.0631	2.9014
qe (exp) (mg g^{-1})	0.4779	0.6037	1.6001	2.2555	0.4779	0.6037	1.6001	2.2555
k	0.0568	0.03728	0.0583	0.0539	0.1072	0.0205	0.0277	0.0191

Table 6
First-order rate constant for photocatalysis using SA/TiO_2 (20 %).

	10 mg/L	15 mg/L	20 mg/L
m	−0.0233	−0.0224	−0.0193
b	1.9047	2.6509	2.8686
r^2	0.9555	0.9959	0.9982
k_{app}	0.0233	0.0224	0.0193

$$In\frac{C}{C_0} = \quad -k_{app}t \tag{7}$$

C_0 = initial concentration of CIP
C = CIP concentration at time t
k_{app} = apparent first-order rate constant (min^{-1})

As shown in Fig. 6, the linearity of the plot confirms that the degradation of CIP by the SA/TiO_2 (20 %) hydrogel is a first-order reaction (Table 6). The calculated rate constants (0.0238, 0.0224, and 0.0193 min^{-1} for CIP concentrations of 10, 15 and 20 mg/L respectively) demonstrate the efficiency of the degradation process across all tested concentrations (Table 5). The rate constants are similar among all CIP concentrations. The Langmuir–Hinshelwood (L–H) model states that

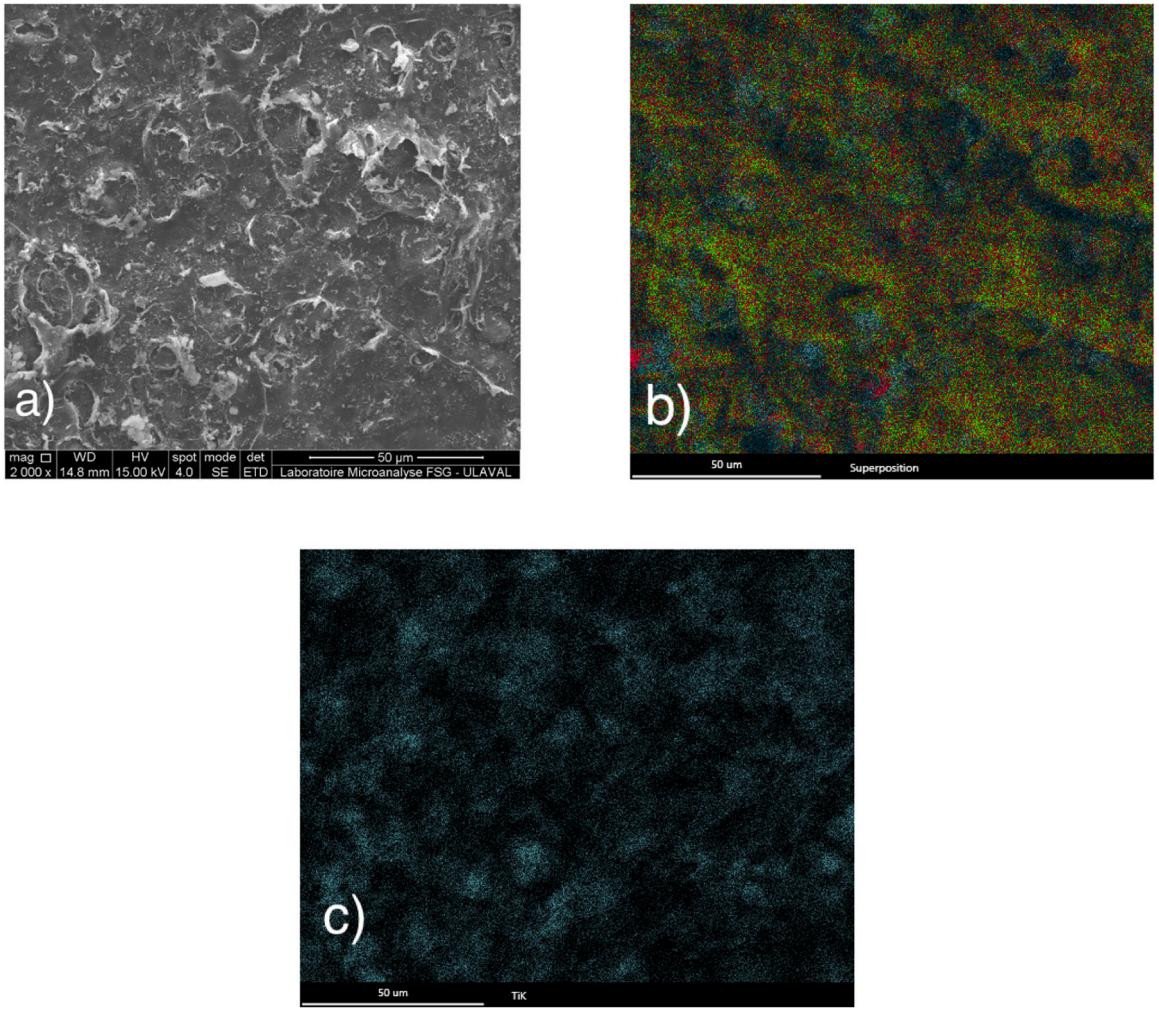

Fig. 10. SEM/EDS elemental mapping SA/TiO_2 hydrogel beads. a) SEM of SA/TiO_2 (20 %) hydrogel without treatment, b) elemental distribution of Ti, C, O, Na and Ca of SA/TiO_2 hydrogel, c) Ti distribution.

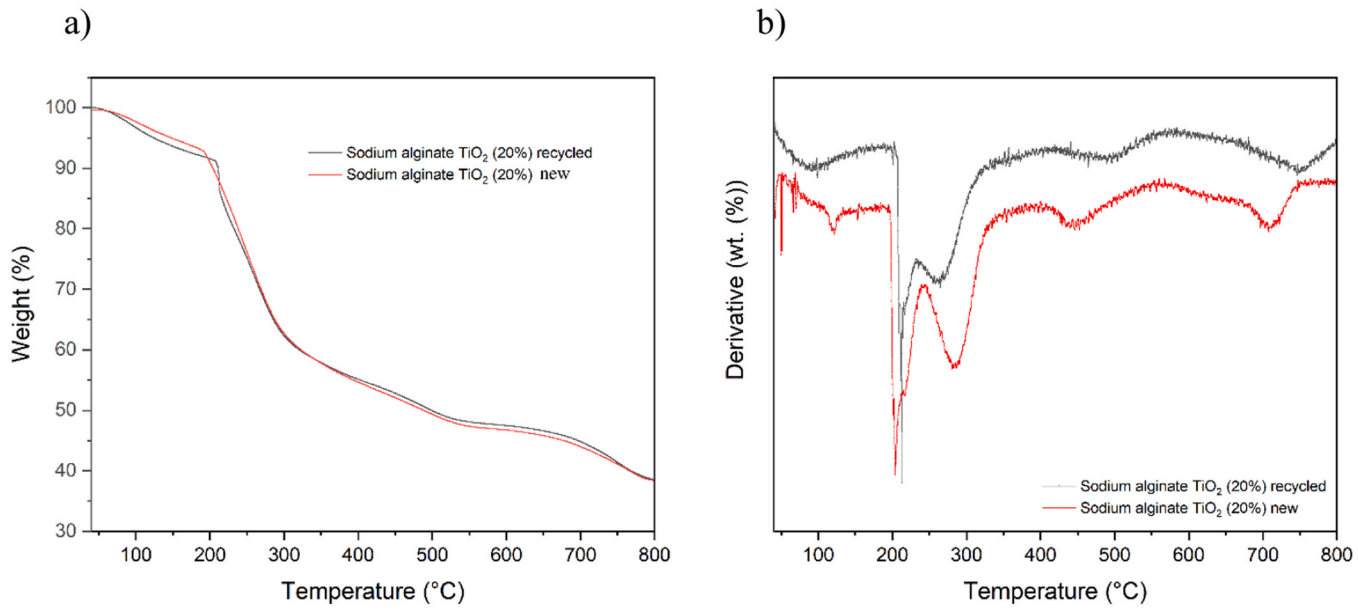

Fig. 11. a) TGA and b) derivative of new and recycled SA/TiO_2 (20 %) used in CIP degradation.

the fraction of catalyst that is occupied by the substrate impacts the degradation rate. This effect is particularly important at high concentrations, where the catalyst is saturated by the substrate, following a zero order equation, while at low concentrations such the ones tested in this study, a first-order model can fit properly the degradation kinetics [55]. Nonetheless, the high removal efficiencies of 99.85, 99.50 and 99.73 % for CIP concentrations of 10, 15, and 20 mg/L after 300 min of light exposure underscore the hydrogel's effectiveness for CIP degradation, making it a promising candidate for water treatment applications.

3.7. Recyclability

The SA/TiO_2 (20 %) hydrogel beads were recycled three times to assess their reusability and stability in adsorbing and degrading CIP (Fig. 7). The recyclability results indicate that the photodegradation efficiency remained stable across all the cycles, with a notable improvement in the adsorption phase. This improvement is likely due to the formation of new pores in the hydrogel matrix structure through the photocatalysis process, as observed in SEM analysis (Fig. 8b). Brunauer-Emmett-Teller (BET) was carried out to observe the changes in the surface area of SA/TiO_2 hydrogel bead comparing the composite without treatment vs recycled. The surface area increased from 1.23 m^2/g to 1.60 m^2/g, and an increase in the average pore size from 262.5 Å to 375.6 Å. These newly formed pores exposed additional active sites, which increased the adsorption efficiency of CIP from 10.14 % in the first cycle to 31.95 % by the third cycle. Despite their good efficiency, the creation of pores can have a negative impact due to the loss of catalyst by leaching and degradation of the hydrogel matrix. Overall, the SA/TiO_2 beads demonstrated good photostability during the three tested cycles and increased their effectiveness for adsorption.

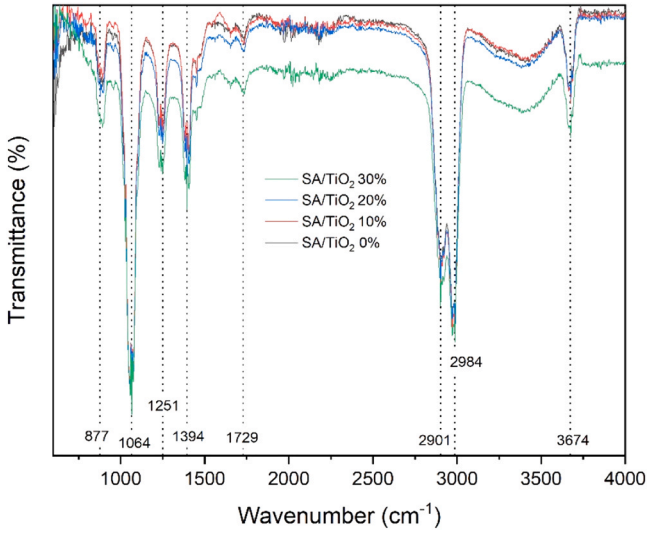

Fig. 12. FT-IR of SA/TiO_2 hydrogel beads loaded at various concentrations of TiO_2.

3.8. Characterization of SA/TiO_2 hydrogel beads

X-ray diffraction revealed the characteristic peaks of TiO2 in both the anatase and rutile phases. Peaks were observed at $2\theta = 29.5°$, 43.2°, 45.1°, and 56.4°, corresponding to the (101), (004), (202), and (211) planes of the anatase phase, respectively. Additionally, peaks at $2\theta = 32.0°$, 42.2°, 45.1°, 64.1°, and 66.9° were observed, corresponding to the (110), (101), (200), (211), and (220) planes of the rutile phase. The composition of TiO_2 was 90.3 of anatase and 9.7 % rutile [56]. No changes were detected in the phases after reaction (Fig. 8).

The morphology of SA/TiO_2 (20 %) hydrogel beads, both before and after use, was studied using SEM (Fig. 9). The SA/TiO_2 (20 %) hydrogel beads exhibited a spherical shape both before and after use. The beads had dimensions ranging between 2 and 3 mm. Prior to adsorption tests, the SA/TiO_2 beads displayed a smooth surface (Figs. 9a and 9c). However, after three cycles of use (Figs. 9b, 9d, and 9f), the hydrogel matrix exhibited significant porosity. Upon magnification of the pores, particle agglomeration was observed on the surface and within the pores, which is likely TiO_2. The TiO_2 agglomerations were also observed by Kumar et al. [49]. A transversal cut at the center of the SA/TiO_2 (20 %) hydrogel bead was conducted to observe the inner layers of the recycled SA/TiO_2 (20 %) bead (Fig. 9e). The presence of interconnected channels was observed. SEM/EDS analysis was performed at 15 kV to observe the elemental distribution of C, O, Na, Ca and Ti (Fig. 10). These results confirmed a homogeneous distribution of Ti in the SA/TiO_2 (20 %) hydrogel bead as well as for C, O, Na and Ca.

3.9. Thermal stability analysis of SA/TiO_2 beads

Dried SA/TiO_2 (20 %) were analyzed by TGA to assess their thermal stability under an inert atmosphere (N_2) (Fig. 11). The thermal stability of SA/TiO_2 (20 %) changed for the recycled samples. Four stages of thermal degradation were identified in both samples, new and recycled. The first stage was from 60 °C to 150 °C, the second stage from 200 °C to 325 °C, the third from 425 °C to 550 °C, and the fourth from 700 °C to 800 °C. The first stage can be explained by the evaporation of water adsorbed by the hydrogel in which the hydrogel lost about 10 % of mass. The second stage occurred due to the destruction of the rings of the polysaccharide SA with a mass loss of around 35 %. For the third stage, the change of SA to sodium carbonate occurred, and finally, for the fourth stage, only TiO_2, calcium and sodium carbonate remained in the sample[57–59]. As it can be observed on Fig. 11b, the thermal stability changed slightly on the recycled SA/TiO_2 (20 %) beads after 3 times of use. This can be due to the mass loss by the photocatalytic process since there is a reduction of the final mass of 3.16 % between the new SA/TiO_2 (20 %) and the recycled SA/TiO_2 (20 %). Probably, the formation of pores allowed some TiO_2 to leach into the media.

FT-IR spectroscopy was used to investigate the interactions between the sodium alginate and TiO_2 catalyst during the hydrogel preparation (Fig. 12). The spectra generally showed similar shapes across different TiO_2 proportions, with variations primarily in peak intensities. Peaks bellow 800 cm^{-1} are attributed to TiO_2 bonding, specifically to the vibrational modes of Ti-O-C and Ti-O-Ti[31], [60]. Notably, the peak at 877 cm^{-1} is more pronounced in samples with a higher concentration of TiO_2.

Peaks in the range of 1015–1300 cm^{-1} are attributed to SA, corresponding to the bending vibrations of O-C-H and C-C-H[61]. The peak at 1394 cm^{-1} is associated with the symmetric stretching vibration of the carboxylate group (COO^-) in SA, as well as the peak observed at 1403 cm^{-1}. Additionally, the carboxylate group is evident in the range of 1600–1700[62]. Peaks at 2901 and 2984 cm^{-1} result from C-H stretching and the presence of -CH and OH-[60,63]. The peaks between 3200 and 3550 cm^{-1} are related to hydrogen (-H) and hydroxyl groups (-OH) associated with the pyranose ring in SA[61].

4. Conclusion

The adsorption and degradation of CIP by the SA/TiO_2 composite hydrogels were evaluated in batch using the optimal conditions for CIP degradation derived from an experimental design. The experiments were divided into two phases: an adsorption phase (60 min) and a photocatalysis phase (up to 360 min). Given that CIP is a zwitterionic molecule, its behavior changed with respect to pH. In this study, the most favorable conditions for CIP adsorption were found at acidic pH, which can be attributed to hydrogen bonding between the carboxylic groups of CIP and sodium alginate. However, a reduction in CIP degradation was observed under acidic conditions, likely due to the reduced availability of OH^- groups necessary to generate •OH radicals during photocatalysis. As a result, the study concluded that optimal CIP degradation occurred in nearly neutral conditions. For practicality, the experiments were conducted at the pH of DI water, achieving 100 % CIP degradation after 60 min of adsorption and 300 min of photocatalysis.

Further studies should focus on adsorption-photocatalysis flow reactions to scale-up, considering factors such as UV light source, reactor design that allows light transmission, and optimal reactor dimensions.

CRediT authorship contribution statement

Tavares Jason Robert: Writing – review & editing, Supervision, Resources, Methodology, Investigation, Funding acquisition, Formal analysis, Conceptualization. **Hernandez Monroy Luis:** Writing – original draft, Methodology, Investigation, Conceptualization. **Dumont Marie-Josée:** Writing – review & editing, Validation, Supervision, Resources, Project administration, Methodology, Investigation, Funding acquisition, Conceptualization.

Declaration of Competing Interest

The authors declare that they have no known competing financial interests or personal relationships that could have appeared to influence the work reported in this paper.

Acknowledgements

The authors acknowledge the Fonds de Recherche du Québec – Nature et Technology (FRQNT), and the Canada Research Chair in Biomass Valorization (to M.-J. D.) for the financial support.

Appendix A. Supporting information

Supplementary data associated with this article can be found in the online version at doi:10.1016/j.jece.2025.115868.

Data availability

Data will be made available on request.

References

[1] I.C. Stanton, A.K. Murray, L. Zhang, J. Snape, W.H. Gaze, Evolution of antibiotic resistance at low antibiotic concentrations including selection below the minimal selective concentration, Commun. Biol. 3 (1) (2020) 467, https://doi.org/10.1038/s42003-020-01176-w.
[2] B. Huerta, et al., Presence of pharmaceuticals in fish collected from urban rivers in the U.S. EPA 2008–2009 national rivers and streams assessment, Sci. Total Environ. 634 (2018) 542–549, https://doi.org/10.1016/j.scitotenv.2018.03.387.
[3] O.I. González Peña, M.Á. López Zavala, H. Cabral Ruelas, Pharmaceuticals market, consumption trends and disease incidence are not driving the pharmaceutical research on water and wastewater, Int. J. Environ. Res. Public. Health 18 (5) (2021) 2532, https://doi.org/10.3390/ijerph18052532.
[4] N. Kumar, H. Mittal, S.M. Alhassan, S.S. Ray, Bionanocomposite hydrogel for the adsorption of dye and reusability of generated waste for the photodegradation of ciprofloxacin: a demonstration of the circularity concept for water purification, ACS Sustain. Chem. Eng. 6 (12) (2018) 17011–17025, https://doi.org/10.1021/acssuschemeng.8b04347.
[5] E.S. Elmolla, M. Chaudhuri, Photocatalytic degradation of amoxicillin, ampicillin and cloxacillin antibiotics in aqueous solution using UV/TiO2 and UV/H2O2/TiO2 photocatalysis, Desalination 252 (2010) 46–52, https://doi.org/10.1016/j.desal.2009.11.003.
[6] P. Kovalakova, L. Cizmas, T.J. McDonald, B. Marsalek, M. Feng, V.K. Sharma, Occurrence and toxicity of antibiotics in the aquatic environment: A review, Chemosphere 251 (2020) 126351, https://doi.org/10.1016/j.chemosphere.2020.126351.
[7] P. Lorenzo, et al., Antibiotic resistance in urban and hospital wastewaters and their impact on a receiving freshwater ecosystem, Chemosphere 206 (2018) 70–82, https://doi.org/10.1016/j.chemosphere.2018.04.163.
[8] M. LeBel, Ciprofloxacin: chemistry, mechanism of action, resistance, antimicrobial spectrum, pharmacokinetics, clinical trials, and adverse reactions, Pharmacother. J. Hum. Pharmacol. Drug Ther. 8 (1) (1988) 3–30, https://doi.org/10.1002/j.1875-9114.1988.tb04058.x.
[9] A.F.C. Leonard, et al., Exposure to and colonisation by antibiotic-resistant *E. coli* in UK coastal water users: environmental surveillance, exposure assessment, and epidemiological study (Beach Bum Survey), *Environ. Int.*,114 (2018) 326–333, https://doi.org/10.1016/j.envint.2017.11.003.
[10] L. Liu, Z.Y. Gao, X.P. Su, X. Chen, L. Jiang, J.M. Yao, Adsorption removal of dyes from single and binary solutions using a cellulose-based bioadsorbent, ACS Sustain. Chem. Eng. 3 (3) (2015) 432–442, https://doi.org/10.1021/sc500848m.
[11] J.S. Im, B.C. Bai, S.J. In, Y.-S. Lee, Improved photodegradation properties and kinetic models of a solar-light-responsive photocatalyst when incorporated into electrospun hydrogel fibers, J. Colloid Interface Sci. 346 (1) (2010) 216–221, https://doi.org/10.1016/j.jcis.2010.02.043.
[12] H. Zhu, Z. Li, J. Yang, A novel composite hydrogel for adsorption and photocatalytic degradation of bisphenol A by visible light irradiation, Chem. Eng. J. 334 (2018) 1679–1690, https://doi.org/10.1016/j.cej.2017.11.148.
[13] X. Wang, X. Li, X. Zhao, C. Li, X. Song, P. Zhang, P. Huo, X. Li, A review on heterogeneous photocatalysis for environmental remediation: from semiconductors to modification strategies 43 (2) (2022) 178–214, https://doi.org/10.1016/S1872-2067(21)63910-4.
[14] Q. Wang, et al., The preparation of BiOCl photocatalyst and its performance of photodegradation on dyes, Mater. Sci. Semicond. Process. 17 (2014) 87–93, https://doi.org/10.1016/j.mssp.2013.08.018.

[15] F. Wang, X. Yu, M. Ge, S. Wu, One-step synthesis of TiO2/γ-Fe2O3/GO nanocomposites for visible light-driven degradation of ciprofloxacin, Chem. Eng. J. 384 (2020) 123381, https://doi.org/10.1016/j.cej.2019.123381.

[16] A.S. Al-Wasidi, Utilisation of adsorption/photocatalytic method for efficient removal of acid orange 8 dye from aqueous media using a novel hydrogel/Fe2O3 composite, Int. J. Environ. Anal. Chem. 103 (17) (2021) 5746–5758, https://doi.org/10.1080/03067319.2021.1942864.

[17] Y. Yue, X. Wang, Q. Wu, J. Han, J. Jiang, Highly recyclable and super-tough hydrogel mediated by dual-functional TiO2 nanoparticles toward efficient photodegradation of organic water pollutants, J. Colloid Interface Sci. 564 (2020) 99–112, https://doi.org/10.1016/j.jcis.2019.12.069.

[18] D. Arikal, A. Kallingal, Photocatalytic degradation of azo and anthraquinone dye using TiO2/MgO nanocomposite immobilized chitosan hydrogels, Environ. Technol. 42 (15) (2021) 2278–2291, https://doi.org/10.1080/09593330.2019.1701094.

[19] D. Atanasova, M. Irikova, D. Staneva, I. Grabchev, Design of a composite based on polyamide fabric-hydrogel-zinc oxide particles to act as adsorbent and photocatalyst, Materials 15 (19) (2022), https://doi.org/10.3390/ma15196649.

[20] F. Chen, W. An, Y. Li, Y. Liang, and W. Cui, "Fabricating 3D porous PANI/TiO2–graphene hydrogel for the enhanced UV-light photocatalytic degradation of BPA," *Appl. Surf. Sci.*, 427 (2028), pp. 123–132, doi: 10.1016/j.apsusc.2017.08.146.

[21] H. Maleki-Ghaleh, et al., Highly efficient magnesium ferrite/graphene nano-heterostructure for visible-light photocatalytic applications: experimental and first-principles DFT studies, Sustain. Mater. Technol. 42 (2024) e01159, https://doi.org/10.1016/j.susmat.2024.e01159.

[22] X. Huang, S. Wu, S. Tang, L. Huang, D. Zhu, Q. Hu, Photocatalytic hydrogel layer supported on alkali modified straw fibers for ciprofloxacin removal from water, J. Mol. Liq. 317 (2020) 113961, https://doi.org/10.1016/j.molliq.2020.113961.

[23] M.N. Abellán, B. Bayarri, J. Giménez, J. Costa, Photocatalytic degradation of sulfamethoxazole in aqueous suspension of TiO2, Appl. Catal. B Environ. 74 (3) (2007) 233–241, https://doi.org/10.1016/j.apcatb.2007.02.017.

[24] M. Sioi, A. Bolosis, E. Kostopoulou, I. Poulios, Photocatalytic treatment of colored wastewater from medical laboratories: photocatalytic oxidation of hematoxylin, J. Photochem. Photobiol. Chem. 184 (1) (2006) 18–25, https://doi.org/10.1016/j.jphotochem.2006.03.028.

[25] Z. Rui, S. Wu, C. Peng, H. Ji, Comparison of TiO2 Degussa P25 with anatase and rutile crystalline phases for methane combustion, Chem. Eng. J. 243 (2014) 254–264, https://doi.org/10.1016/j.cej.2014.01.010.

[26] J.-L. Zhu, S.-P. Chen, W. Lin, H.-D. Huang, Z.-M. Li, Cellulose mineralization with in-situ synthesized amorphous titanium dioxide for enhanced adsorption and auto-accelerating photocatalysis on water pollutant, Chem. Eng. J. 456 (2023) 141036, https://doi.org/10.1016/j.cej.2022.141036.

[27] A. Pardo *et al.*, "Self-regenerating photocatalytic hydrogel for the adsorption and decomposition of methylene blue and antibiotics in water," *Environ. Technol. Innov.*, 11 (2028), pp. 321–327, doi: 10.1016/j.eti.2018.06.005.

[28] K. Zhao, et al., Adsorption and photocatalytic degradation of methyl orange imprinted composite membranes using TiO2/calcium alginate hydrogel as matrix, Catal. Today 236 (2014) 127–134, https://doi.org/10.1016/j.cattod.2014.03.041.

[29] S. Wan, W. Zhao, D. Xiong, S. Li, Y. Ye, L. Du, Novel alginate immobilized TiO $_2$ reusable functional hydrogel beads with high photocatalytic removal of dye pollutions, J. Polym. Eng. 42 (10) (2022) 978–985, https://doi.org/10.1515/polyeng-2022-0017.

[30] Y. Qing, Y. Li, Z. Guo, Y. Yang, W. Li, Photocatalytic Bi2WO6/pg-C3N4-embedded in polyamide microfiltration membrane with enhanced performance in synergistic adsorption-photocatalysis of 17β-estradiol from water, J. Env. Chem. Eng. 10 (6) (2022) 108648, https://doi.org/10.1016/j.jece.2022.108648.

[31] K. Zhao, et al., Preparation, characterization and photocatalytic degradation properties of a TiO2/calcium alginate composite film and the recovery of TiO2 nanoparticles, RSC Adv. 4 (93) (2014) 51321–51329, https://doi.org/10.1039/C4RA08102A.

[32] K.T.T. Myint, J.G. Ge, H.J.Y. Niu, J. Chen, Z. Jiao, A separation-free and pizza-structure PAM/GCN/PAA composite hydrogel (PCH) in wastewater treatment at visible light or solar light, Sci. Total Environ. 705 (2020) 135821, https://doi.org/10.1016/j.scitotenv.2019.135821.

[33] "US Pharmacopeia (USP)." Accessed: Jul. 31, 2023. [Online]. Available: ⟨https://www.usp.org/⟩.

[34] J.R. Krishna, B. Naga, and S. Huidrom, "Development and Validation of UV Spectrophotometric method for the Simultaneous estimation of Ciprofloxacin Hydrochloride and Ornidazole in Combined Pharmaceutical Dosage Form," 4 (4) (2014).

[35] "Pharmaceutical pollution of the world's rivers." Accessed: Oct. 18, 2022. [Online]. Available: ⟨https://www.pnas.org/doi/10.1073/pnas.2113947119⟩.

[36] S. Chkirida, et al., Highly synergic adsorption/photocatalytic efficiency of alginate/bentonite impregnated TiO2 beads for wastewater treatment, J. Photochem. Photobiol. Chem. 412 (2021) 113215, https://doi.org/10.1016/j.jphotochem.2021.113215.

[37] S.I. Pechenyuk, The use of the pH at the point of zero charge for characterizing the properties of oxide hydroxides, Russ. Chem. Bull. 48 (6) (1999) 1017–1023, https://doi.org/10.1007/BF02495994.

[38] B. Liu, et al., Adsorption of lead ions by activated carbon doped sodium alginate/sodium polyacrylate hydrogel beads and their in-situ recycle as sustainable photocatalysts, J. Colloid Interface Sci. 645 (2023) 133–145, https://doi.org/10.1016/j.jcis.2023.04.091.

[39] C. Jeong, S. Kim, C. Lee, S. Cho, S.-B. Kim, Changes in the physical properties of calcium alginate gel beads under a wide range of gelation temperature conditions, Foods 9 (2) (2020) 180, https://doi.org/10.3390/foods9020180.

[40] H. Heidarpour, M. Golizadeh, M. Padervand, A. Karimi, M. Vossoughi, M. H. Tavakoli, In-situ formation and entrapment of Ag/AgCl photocatalyst inside cross-linked carboxymethyl cellulose beads: a novel photoactive hydrogel for visible-light-induced photocatalysis, J. Photochem. Photobiol. Chem. 398 (2020) 112559, https://doi.org/10.1016/j.jphotochem.2020.112559.

[41] A. Enesca, L. Isac, The influence of light irradiation on the photocatalytic degradation of organic pollutants, Materials 13 (11) (2020) 2494, https://doi.org/10.3390/ma13112494.

[42] H. Ou, J. Ye, S. Ma, C. Wei, N. Gao, J. He, Degradation of ciprofloxacin by UV and UV/H 2 O 2 via multiple-wavelength ultraviolet light-emitting diodes: effectiveness, intermediates and antibacterial activity, Chem. Eng. J. 289 (2016) 391–401, https://doi.org/10.1016/j.cej.2016.01.006.

[43] D. Li, Y. Meng, J. Li, Y. Song, F. Xu, TiO2/carbonaceous nanocomposite from titanium-alginate coordination compound, Carbohydr. Polym. 288 (2022) 119400, https://doi.org/10.1016/j.carbpol.2022.119400.

[44] Y. Wu, et al., Versatile magnetic adsorbent based on sodium p-styrenesulfonate modified sodium alginate composite for effective capture of antibiotic ciprofloxacin, methylene blue and copper ion, J. Clean. Prod. 373 (2022) 133651, https://doi.org/10.1016/j.jclepro.2022.133651.

[45] A. Allangawi, M.A. Aziz Aljar, K. Ayub, A.A. El-Fattah, T. Mahmood, Removal of methylene blue by using sodium alginate-based hydrogel; validation of experimental findings via DFT calculations, J. Mol. Graph. Model. 122 (2023) 108468, https://doi.org/10.1016/j.jmgm.2023.108468.

[46] L. Jara-Cobos, D. Abad-Delgado, J. Ponce-Montalvo, M. Menendez, M.E. Peñafiel, Removal of ciprofloxacin from an aqueous medium by adsorption on natural and hydrolyzed bentonites, Front. Environ. Sci. 11 (2023), https://doi.org/10.3389/fenvs.2023.1239754.

[47] C.A. Igwegbe, S.N. Oba, C.O. Aniagor, A.G. Adeniyi, J.O. Ighalo, Adsorption of ciprofloxacin from water: A comprehensive review, J. Ind. Eng. Chem. 93 (2021) 57–77, https://doi.org/10.1016/j.jiec.2020.09.023.

[48] F.H. Hussein, Photochemical treatments of textile industries wastewater, ASIAN J. Chem. 24 (12) (2012) 5427–5434. Dec. 2012.

[49] R. Kumar, et al., Integrated adsorption-photocatalytic decontamination of oxytetracycline from wastewater using S-doped TiO2/WS2/calcium alginate beads, Catalysts 12 (12) (2022), https://doi.org/10.3390/catal12121676.

[50] "Ciprofloxacin.", National Library of Medicine, Accessed: Aug. 07, 2024. [Online]. Available: ⟨https://pubchem.ncbi.nlm.nih.gov/compound/2764⟩.

[51] H. Zhu, T. Chen, J. Liu, D. Li, Adsorption of tetracycline antibiotics from an aqueous solution onto graphene oxide/calcium alginate composite fibers, RSC Adv. 8 (5) (2018) 2616–2621, https://doi.org/10.1039/C7RA11964J.

[52] Y. Fei, Y. Li, S. Han, J. Ma, Adsorptive removal of ciprofloxacin by sodium alginate/graphene oxide composite beads from aqueous solution, J. Colloid Interface Sci. 484 (2016) 196–204, https://doi.org/10.1016/j.jcis.2016.08.068.

[53] J. Wang, X. Guo, Adsorption kinetic models: Physical meanings, applications, and solving methods, J. Hazard. Mater. 390 (2020) 122156, https://doi.org/10.1016/j.jhazmat.2020.122156.

[54] M. Nawaz, A.A. Khan, A. Hussain, J. Jang, H.-Y. Jung, D.S. Lee, Reduced graphene oxide-TiO_2/sodium alginate 3-dimensional structure aerogel for enhanced photocatalytic degradation of ibuprofen and sulfamethoxazole, Chemosphere 261 (2020) 127702, https://doi.org/10.1016/j.chemosphere.2020.127702.

[55] M. Abbas, Factors influencing the adsorption and photocatalysis of direct red 80 in the presence of a TiO2: Equilibrium and kinetics modeling, J. Chem. Res. 45 (7-8) (2021) 694–701, https://doi.org/10.1177/1747519821989969.

[56] I. Morad, M.M. El-Desoky, A. Mansour, M. Wasfy, Synthesis, structural and electrical properties of PVA/TiO2 nanocomposite films with different TiO2 phases prepared by sol-gel technique, J. Mater. Sci. Mater. Electron. 27 (2020), https://doi.org/10.1007/s10854-020-04313-7.

[57] F. Liu, et al., Preparation of green sodium alginate adsorption membrane and its high adsorption performance for fluoroquinolones antibiotics br, J. Water Process Eng. 49 (2022) 103124, https://doi.org/10.1016/j.jwpe.2022.103124.

[58] M.A. Ibrahim, G.M. Nasr, R.M. Ahmed, N.A. Kelany, Physical characterization, biocompatibility, and antimicrobial activity of polyvinyl alcohol/sodium alginate blend doped with TiO_2 nanoparticles for wound dressing applications, Sci. Rep. 14 (1) (2024) 5391, https://doi.org/10.1038/s41598-024-55818-8.

[59] S. Chandraraj, J. Xavier, Electrochemical and mechanical investigation into the effects of polyacrylamide/TiO2 in polyurethane coatings on mild steel structures in chloride media, J. Mater. Sci. 57 (2022), https://doi.org/10.1007/s10853-022-07483-3.

[60] D. Ma, T. E, S. Yang, Efficient removal of Cu(II) with graphene oxide-titanium dioxide/sodium alginate composite beads: Preparation, characterization, and adsorption mechanism, J. Environ. Chem. Eng. 9 (6) (2021) 106501, https://doi.org/10.1016/j.jece.2021.106501.

[61] H. Shehzad, et al., Modified alginate-chitosan-TiO2 composites for adsorptive removal of Ni(II) ions from aqueous medium, Int. J. Biol. Macromol. 194 (2022) 117–127, https://doi.org/10.1016/j.ijbiomac.2021.11.140.

[62] J. Dai, et al., TiO_2-alginate composite aerogels as novel oil/water separation and wastewater remediation filters, Compos. Part B-Eng. 160 (2019) 480–487, https://doi.org/10.1016/j.compositesb.2018.12.097.

[63] H. Helmiyati and F.W. Dini, "Synthesis and application of nanocomposite based on nano sodium alginate from brown seaweed impregnation TiO2 as a catalyst for synthesis 5-hydroxymethylfurfural from fructose," presented at the Proceedings of the 3rd international symposium on current progress in mathematics and sciences, Bali, Indonesia, 2018, p. 020101. doi: 10.1063/1.5064098.